minerals

MDPI

Article

Crystallization Behaviour of Iron-Hydroxide Sulphates by Aging under Ambient Temperature Conditions

Amalia Jiménez *, Ana Hernández and Manuel Prieto

Department of Geology, University of Oviedo, 33005 Oviedo, Spain; ana.her.rod82@gmail.com (A.H.); mprieto@uniovi.es (M.P.)

* Correspondence: amjimenez@uniovi.es

Received: 11 December 2018; Accepted: 4 January 2019; Published: 5 January 2019

Abstract: The crystallization behaviour of jarosite and schwertmannite has been studied by precipitation-aging experiments performed using different parent-solution concentrations at acidic conditions and ambient temperature. Schwertmannite exhibits low crystallinity and is the only mineral identified during low-concentration (LC) experiments. However, in high-concentration (HC) experiments, a relatively rapid Ostwald ripening process leads to the transformation of schwertmannite into natrojarosite. The presence of sodium modifies the morphology and stability of the obtained phases. TEM observations reveal that schwertmannite particles consist of disoriented nanodomains (~6 nm) spread in an amorphous mass. In contrast, natrojarosite particles exhibit a single-domain, highly crystalline core, with the crystallinity decreasing from core to rim. The thermal behaviour of these phases depends on both their composition and their degree of crystallinity. TG and DTG analyses show that, below 500 °C, the amount of structural water is clearly higher in schwertmannite than in natrojarosite. The present results highlight the role of the ripening processes in epigenetic conditions and could be important in interpreting the formation of jarosite in Earth and Martian surface environments.

Keywords: jarosite; schwertmannite; morphology; precipitation; decomposition behaviour; supergene

1. Introduction

Fe-bearing minerals such as oxides, hydroxides, oxyhydroxides, and sulphates are common in the Earth's lithosphere, hydrosphere, atmosphere and biosphere, where they participate in diverse biogeochemical processes [1]. The weathering of ferrous sulphide minerals (pyrite, chalcopyrite, pyrrhotite, mackinawite, marcasite and arsenopyrite) is of particular interest because it controls the formation of large amounts of insoluble and fairly soluble Fe-bearing secondary phases (mainly ferric hydroxides and hydroxysulphates) through processes mediated by bacterial activity in both natural systems and industrial wastewaters [2]. Typically, these secondary minerals are formed by Fe(III), are poorly soluble [3] and (with the exception of schwertmannite and ferrihydrite) have a well-developed crystalline structure. Some of these ferric hydroxysulphates, as jarosite, are of significant importance not only in near-surface natural environments but also in metallurgical and industrial processes [4,5]. Furthermore, the increasing use of iron sulphates in the industry, to develop new materials such as pigments, magnetic materials, and catalysers enhance the interest of mine ferric oxyhydroxysulphates [6–8].

Precipitation of ferric oxyhydroxysulphates plays a key role in geochemical processes occurring in supergene exploitable deposits. The implication of iron-bearing minerals in both early weathering processes and hydrothermal mineral genesis is one of the reasons of their prospection and mining

importance [9]. The mobility and surficial distribution of Fe-bearing minerals provide evidences for understanding the nature of hydrothermally altered rocks and their associated mineral deposits and how supergene enrichment occurs [9]. In particular, the precipitation of metastable phases such as schwertmannite facilitate the adsorption of heavy metals in acid mine drainage (AMD) systems [10] because of its high specific surface area and result in significant residual accumulations of these potentially toxic constituents in epigenetic conditions. The flexibility of the jarosite structure, which makes minerals in this group a sink for toxic metals, together with their low solubility, determine their environmental significance [11–13]. However, the fact that poorly crystalline Fe(III)-oxy-hydroxy-sulphates transform into other more crystalline phases [10,14–16] illustrates the complex role of iron oxides in controlling the mobility of pollutants in natural waters. Although remediation of mine sites is an engineering concern, designing a remediation plan without understanding the hydrogeochemical behaviour of contaminants can lead to ineffective and excessively costly remediation.

Presence of iron compounds showing different crystallinity degrees such as schwertmannite ($Fe_8O_8(OH)_6(SO_4)_2 \cdot nH_2O$) and jarosite ($KFe_3(SO_4)_2(OH)_6$) have been identified on the Martian surface by spectroscopies analyses [17–20]. Although Mars surface seems to be dominated by hydronium- and K-jarosites, the presence of Na-jarosite is also possible after weathering of Na feldspar bearing basalt [21]. These contributions have generated an increasing interest in the planetary geology community, even more interest than the dominant silicate materials, in order to find indicators of water-limited chemical weathering and different mineral formation pathways on that planet [22]. Many of the Martian bright regions seems to be covered by ferricretes and fine-grained "soil", rich in silicates and nanophase Fe minerals [19,23]. The existence of gossans and related ferricretes on Earth as aqueous weathering products could be an evidence for similar episodes of weathering on Mars under an earlier climatic regime that could be warmer and wetter [24]. These meltwaters are generally thought to have been acidic [25] and might therefore have been similar to many epigenetic deposits on Earth.

Although different jarosite-type compounds have been synthesized by precipitation at temperatures close to 100 °C, the genesis of these minerals at ambient conditions needs to be studied in depth to understand both the hydrogeochemical processes and the phase transformations involved in the formation of supergene enrichment deposits. In this framework, the present work focuses on the study of the crystallization behaviour of ferric-bearing sulphates at ambient temperature and acidic conditions. The influence of the concentration of common ions on Earth's surface (i.e., Na^+) in the precipitation, crystallinity and composition of phases formed during aging experiments was studied with a combination of XRD, SEM and TEM. The decomposition behaviour was also studied under non-isothermal conditions by thermogravimetry, and the obtained results were correlated with the results of the XRD study.

2. Materials and Methods

2.1. Precipitation Experiments

Iron hydroxysulphates were precipitated and aged by mixing two reactants ($Fe_2(SO_4)_3 \cdot xH_2O$ and NaOH) at ambient conditions. Previously, aqueous solutions were prepared with analytic grade (Panreac®) reactants and deionized Milli-Q® water being stirred for one hour and then, stored in a refrigerator until use. A set of experiments were carried out by mixing the most concentrated solutions of 0.25 M of $Fe_2(SO_4)_3$ and 1 M of NaOH (60:40 ratio) to obtain 100 mL of aqueous solutions (HC-20). Another set of experiments were conducted by adding 50 mL of each parent solution (0.16 M of $Fe_2(SO_4)_3$ and 0.5 M of NaOH) with the lowest concentration (LC-20). In both experiments, the mixture was stirred at 250 rpm over 1 day and 28 days. After mixing parent solutions, the reaction cells were sealed with a cover to avoid evaporation and they were kept under constant stirring (250 rpm) in a thermostat cabinet (20 ± 0.5 °C). Independent experimental runs were aged during 1 day and 28 days

for each initial solution (HC-20 and LC-20). At the beginning and at the end of each experiment, the pH was measured with a combination electrode (Ross-Thermo-Orion-810200, Thermo Fisher Scientific, Waltham, MA, USA) and a digital pH-meter (CyberScan-pH-2100, Thermo Fisher Scientific, Waltham, MA, USA). After the corresponding reaction period, solid and liquid phases were separated by centrifugation in a Selecta Meditronic equipment (JP Selecta, Barcelona, Spain) during 5 min at 3000 rpm. In the case of the LC experiments, a tiny solid was retained in the filter membrane, and therefore, a second cycle of centrifugation during 5 min at 3000 rpm was applied to obtain a total separation of aqueous solution and solid phases. The precipitates were dried at room temperature in a desiccator to avoid dehydration and aqueous solutions were stored in polypropylene tubes and refrigerated. After drying period, the solids were gently crushed by hand using an agate mortar to a fine powder. Every experiment was repeated three times in order to check the reproducibility of the results.

Iron and sodium dissolved were analysed with ICP-OES (Perkin-Elmer-Optima-3300-DV, PerkinElmer, Waltham, MA, USA) and sulphate was analysed by IC (Metrohm Compact IC 761, Metrohm AG, Herisau, Switzerland). Previously, the samples were diluted and filtered (0.45 μm). The aqueous solutions were modelled using the geochemical code PHREEQC [26] to calculate activities of different chemical species and saturation indexes (SI) with respect to relevant solid phases at the beginning of the experiments. The wateq.dat database was completed with the thermodynamic solubility product of schwertmannite ($Ksp = 10^{-5.28}$) [27].

2.2. Characterization of Phases

A representative sample of each precipitate was selected to study the composition, morphology and crystallinity of the precipitate. Characterization of the solid phases formed during aging and the evolution of its crystallinity was stated by Powder X-ray diffraction (XRD). The diffraction patterns were collected in a Philips X'Pert-PRO automatic diffractometer (Malvern Panalytical Ltd., Malvern, UK) using CuKα radiation in the 2θ range from 5° to 60° with a step size of 0.02°. The calibration of the diffractometer was made using an external silicon (Si) standard before measurements. Indexing of the main reflections were made using the crystallographic analysis tools of the computer program X'Pert HighScore Plus (©2008, Malvern Panalytical Ltd., Malvern, UK). Scanning electron microscopy (SEM) micrographs were collected under a JEOL6610LV microscope (JEOL, Ltd., Akishima, Japan), after coating the samples with gold in a Balzers SCD004 sputter. Both secondary and backscattered electron images were obtained, to observe the morphology of the solids and to discard possible compositional inhomogeneities within the precipitates. High resolution transmission electron microscopy (HRTEM) images and selected-area electron diffraction (SAED) patterns were obtained to verify the degree of crystallinity at the nanoscale using a JEOL JEM-2100 electron microscope (JEOL, Ltd., Akishima, Japan), operating at 200 kV. Fine powder of the samples was dispersed in ethanol and dropped onto carbon coated copper grids and then allowed to air-dry.

2.3. Thermal Behavior

Representative samples of solids obtained at HC and LC series were selected to study their thermal behaviour. TG and DTG analyses were performed using a Metter Toledo TGA/SDTA 851 thermal analyser (METTLER TOLEDO, Columbus, OH, USA). All measurements were performed for the 25–1000 °C temperature range at a heating rate of 10 °C·min^{-1} in a dynamic atmosphere, using a nitrogen flow rate of 50 mL·min^{-1}. The temperature and weight precision of the apparatus were ±0.25 K and ±1 μg, respectively. A Pfeiffer Vacuum ThermoStar™ GSD301T mass spectrometer (Pfeiffer Vacuum Technology AG, Aßlar, Germany) was used to analyse the gas phases released during the TG study. The masses 18 (H_2O) and 48 (SO) and 64 (SO_2) were tested by using a detector C-SEM, operating at 1400 V, with a time constant of 0.5 s.

3. Results and Discussion

3.1. Evolution of the Aqueous Solution

At the beginning of the experiments, a colloidal mixture of dark brown colour is obtained, which has been dispersed within a few hours of the start of the reaction. At the same time, changes of colour to brown-reddish or yellowish go together with the decreases of Fe, Na, and sulphate and pH level (Table 1). The most pronounced decrease takes place during the first day of aging and then the ion concentration and pH values fall slowly until the end of the reaction period. These results indicate that the evolution of the physic-chemical properties of aqueous phases is related to the different concentration of the parent solutions and the nature of the precipitates obtained during aging at various reaction times.

Table 1. Concentration of Fe, Na, sulphate and pH at the beginning (pHi) and at the end (pHf) of each reaction period.

Reference	pHi	pHf	Fe (mM)	Na (mM)	SO_4 (mM)
LC-1d	2.69	2.25	0.013	0.209	0.120
LC-28d	2.71	2.28	0.011	0.162	0.100
HC-1d	2.92	2.42	0.138	0.273	0.267
HC-28d	2.90	2.28	0.073	0.219	0.202

3.2. Nature and Morphology of Solid Phases

The powder XRD diagrams of the solids obtained for LC experiments (Figure 1) show broad and low intensity reflections that reveal the low crystallinity of the precipitates at the beginning and at the end of reaction time (LC-1d and LC-28d). It is well known that the characterization of poorly crystalline phases is not straightforward using conventional powder XRD because of the lack of discernible Bragg reflections. However, the diffraction pattern obtained for these solids deserves to be studied because they are certainly not X-ray amorphous. The diffractogram obtained in the early stage (1 day) shows two broad peaks at 2θ of ~35° and ~61° that might match not only with the least crystalline form of ferrihydrite (two-line ferrihydrite) [28,29] but also with schwertmannite [30]. The low crystallinity of both ferrihydrite and schwertmannite, is related with the small size of the coherent diffraction domains as well as with structural disorder and vacancies in their structures [31]. On one hand, ferrihydrite is an iron oxyhydroxide, with a rough formula $Fe_{10}O_{14}(OH)$, that is only stable under near-neutral pH values at ambient temperature [27,29,32]. On the other hand, schwertmannite is a ferric oxyhydroxysulphate ($Fe_8O_8(OH)_{5.5}(SO_4)_{1.25}$), which was recognized as a mineral (PDF 47-1775) in spite of its meta-stability [10,14]. Caraballo et al. [33] described schwertmannite as a polyphasic nano-mineral that always precipitates under pH < 4.71 values. As mentioned above, the aqueous solution is acidic during the overall reaction times and hence, the presence of ferrihydrite ($Fe_{10}O_{14}(OH)$) at the beginning of the experiments can be discarded.

The diffractograms obtained for solids precipitates in HC experiments (Figure 1) reveals that a poorly crystalline phase precipitates at the beginning of the experiments (HC-1h). In a first approach, the broad reflections displayed in the diffraction pattern obtained at the beginning seem similar to that obtained in LC experiments. However, a detailed study displays broad reflections coexisting with incipient reflections at 2θ of ~17.61°, ~28.65°, and ~29.29° that indicate the existence of a phase with some degree of crystallinity. The XRD patterns of the precipitates obtained at the end of reaction time shows that those incipient reflections become more apparent as the reaction times passes by (HC-28d). These reflections match with the main XRD reflections (012, 021 and 113) of natrojarosite ($NaFe_3(SO_4)_2(OH)_6$), which crystallize in the rhombohedral system (*R3m* Spatial Group No 160). It must be pointed that any other crystalline phases (hematite, goethite, etc.) have not been identified in the precipitates. Thus, the precipitates obtained after aging in HC experiments can be identified as natrojarosite-like compounds.

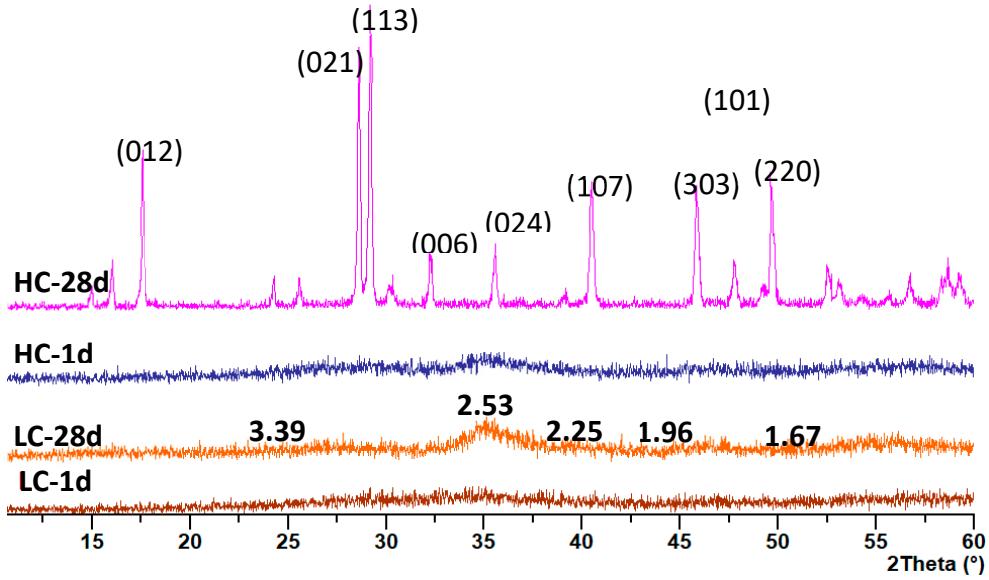

Figure 1. X-ray diffractograms of the solid phases obtained during aging experiments performed with low concentration (LC) and high concentration (HC). Numbers give d-values (Å) for the diffraction peaks of schwertmannite and (hkl) planes are identified for natrojarosite.

Figure 2 shows the electron images of representative solids obtained in LC experiments. The secondary electron images (Figure 2a) shows grains of size higher of 50 μm coexisting with grains of lower dimension (<1 μm), which corresponds to the fragments obtained by hand crushing the aggregated of colloidal particles obtained after drying. The conchoidal fractures of particles is in agreement with the poorly crystalline nature of schwertmannite. The EDS analysis indicates that all the solids (LC experiments) are composed of iron, sulphur, oxygen and sodium. Although these analyses are semi-quantitative, they give an approximation of the chemical composition and confirm that a Na-schwertmannite-like compound ($(NaFe)_8O_8(OH)_6(SO_4)_2 \cdot nH_2O$) is the most probable phase to precipitate as sodium has been identified by the EDS analysis. The shape and crystallinity degree of the particles obtained has been also studied by means of TEM (Figure 2b). As observed, the particles are individual entities and show flat and irregular shapes with relatively smoothed edges. In addition, the crystallinity is not homogeneous and show nanodomains (~6 nm) disoriented with respect to their neighbours dispersed throughout the sample (Figure 2b). It is worth mentioning that some vacuoles appear on the surface of the particles, which is inherent to the melting of hydroxides after electron beam interaction. The particles or crystal aggregates of schwertmannite seem to be always characterized by a distinctive needle-like or "hedgehog" morphology, which has been widely reported in natural and synthetic precipitates from acid and sulphate-rich waters [30,34,35]. However, the typical spherulites formed by the aggregation of small individual crystals with needle-like morphology of schwertmannite has not been observed in the solids obtained in the present experiments (see Figure 2). It should be stated that the identification of phases using exclusively the habit is not definitive as the morphology of the crystals is not determined only by crystal structure but also by factors as temperature, supersaturation and impurities present in solution during growth [36]. In particular, the capability of schwertmannite to adsorb ions or the formation of surface complexes between iron surface groups and different oxyanions [10,37,38] and the crystal structure of schwertmannite with channels formed by iron octahedral [39] could explain the lack of the typical needle-like morphology of this poorly crystalline phase. The effect of the impurities modifies the kinetic of crystal growth revealing a decrease in the velocity of growth that evolves until reach a period without crystal growth (dead zone) in which growth is entirely blocked [40]. In this case, the adsorption of Na on reactive sites or inside the channels formed by iron octahedral could be responsible for the morphology of schwertmannite particles observed by SEM.

The morphology of HC precipitates evolves with increasing aging (Figure 3). Thus, aggregates of small crystals with shapeless morphology are observed at the beginning of the experiments (HC-1d) while typical rhombohedral morphologies with similar sizes (~1 μm) can be clearly distinguished at the end of the aging experiments (Figure 3a). In addition, TEM images reveal that the natrojarosite particles seem to have a core/shell morphology (Figure 3b). The core of each particle of natrojarosite forms a highly crystalline single domain as evidenced by the periodic atomic arrangement shown in Figure 3b. However, a progressive loss of crystallinity as approaching the edge is observed. Indeed, a lack of defined atomic planes at the 2–3 nm outer shell of the particles is observed.

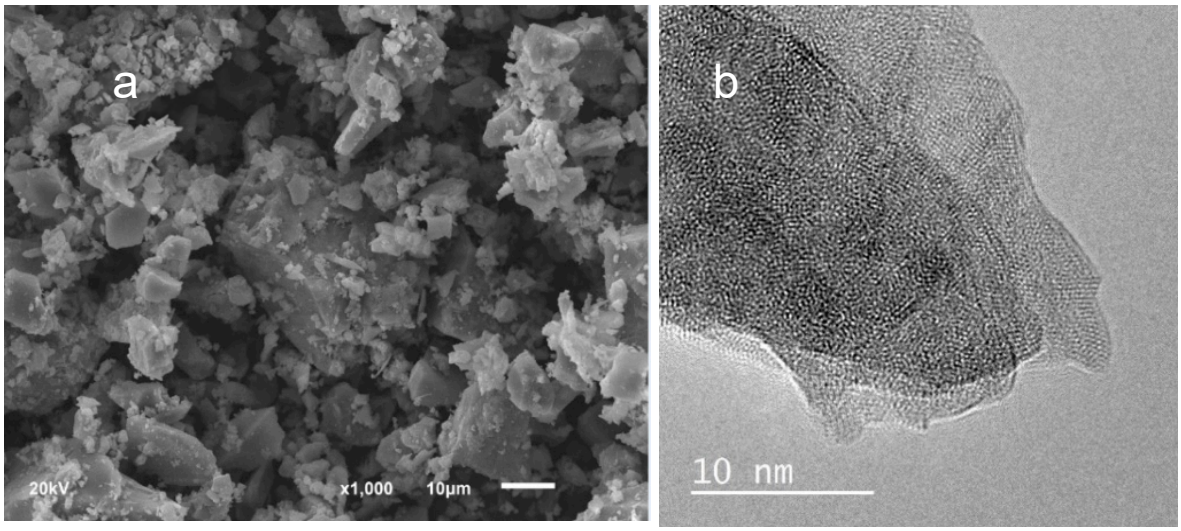

Figure 2. SEM and TEM images showing the morphology (**a**) and nano-domains (**b**) of schwertmannite particles obtained by aging after 28 days of aging (LC-28).

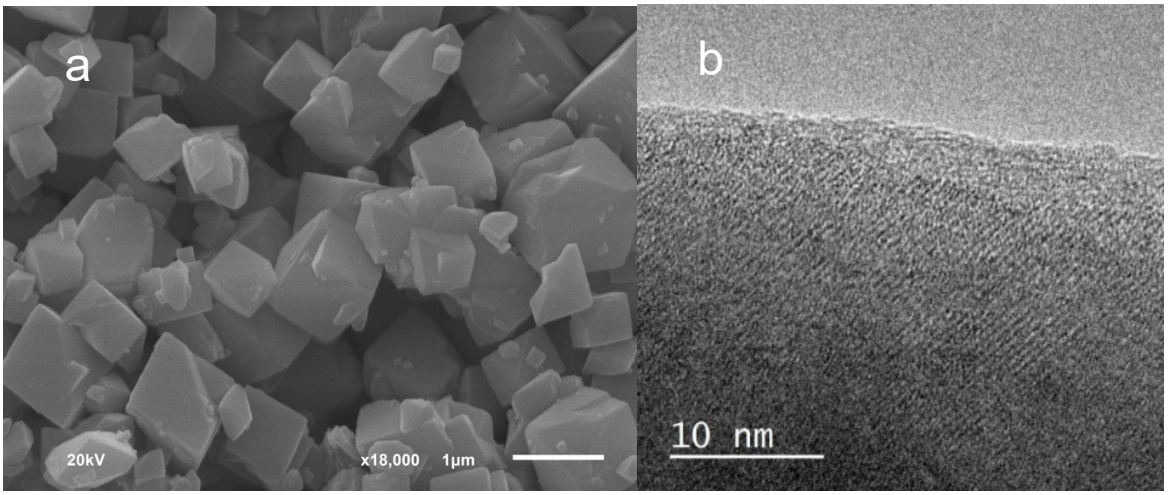

Figure 3. SEM and TEM images showing the rhombohedral shape (**a**) and the core-shell morphology of a single domain (**b**) of natrojarosite obtained by aging after 28 days (HC-28d).

These observations confirm the results obtained by XRD concerning the increasing degree of crystallization of natrojarosite with aging (Figure 1). On the other hand, the lack of rhombohedral morphology of natrojarosite during early stages of aging suggest that crystals are too small to develop that morphology, but these tinny crystals are built by diffraction domains responsible for XRD reflections (Figure 1) at the very early stages of growth. The EDS analyses indicate that both phases, the poorly crystalline and the crystalline ones, are composed of iron, sulphur, oxygen and sodium. The composition of the low crystalline phase is similar to that obtained for the LC solids. In the case

of more crystalline precipitates (HC-28d), EDS analysis yield atomic ratios of 1.4 for Fe/S and 0.3 for Na/Fe, which suggest that iron and sodium contents per unit formula were slightly lower than the stoichiometric ratio (1.5 for Fe/S and 0.33 for Na/Fe) corresponding to jarosite-like compounds ($NaFe_3(SO_4)_2(OH)_6$). As mentioned above, these data can be indicative of partial substitution of sodium by hydronium ions in the alkali position. Consistent with XRD study, the EDS analyses confirm that the crystalline phases are Na-rich members of the $(Na,H_3O)Fe_3(SO_4)(OH)_6$ solid solution.

3.3. The role of Na during Aging

A pe-pH diagram for the main Fe mineral phases has been described by Bigham et al. [32]. These authors propose that jarosite is stable at high-pe and acid sulphate waters (pH lower than 2.5) while schwertmannite can precipitate at higher pH values (between 2.5 and 4.5) but it is unstable relative to goethite over the pH range of 2–6. Caraballo et al. [33] presented a flexible solubility range for schwertmannite (log K_{sp} from 5.8 to 39.5) that permit a better understanding of the distribution of the main Fe mineral phases in nature. With regards to the present experimental conditions and prevailing acidic conditions, the precipitation of iron hydroxide sulphate phases is therefore expected at the beginning of both experiments. The saturation states of the initial aqueous solutions with respect to the phases susceptible to precipitate are in agreement with the identification of schwertmannite and natrojarosite by XRD (Figure 1). Thus, at the very beginning of LC experiments, the solution is clearly saturated with respect to schwertmannite (SI~71) followed by natrojarosite (SI ~14), goethite (SI ~11), and hydronium-jarosite (SI ~9). In the case of HC experiments, the solution is also saturated with respect to schwertmannite (SI ~68), natrojarosite (SI ~15), and hydronium-jarosite (SI ~11) and goethite (SI ~10). In the present experiments, the metastable phase (schwertmannite) appears as initial precipitate (see Figure 1) and its presence can be interpreted as a nanocrystal precursor of other crystalline phases in agreement with Caraballo et al. [33]. These authors [33] propose a thermodynamic model assuming equilibrium between solution, hydrous ferric oxide and schwertmannite to explain the complex precipitation behaviour of the latter polyphasic nano-mineral. Although schwertmannite is the major phase identified at the beginning of both LC and HC experiments, it is assumable that some small nuclei of natrojarosite will be also formed. As mentioned above, a schwertmannite like compound is the only phase identified and its transformation into other more stable phase (jarosite or goethite) has not been observed during the reaction times considered in LC experiments. Thus, the transformation process needs long period of time to reach equilibrium and the reaction of precipitation of schwertmannite could be envisaged as:

$$4Fe_2(SO_4)_3 + 4NaOH + 9.5H_2O \rightarrow Fe_8O_8(OH)_{5.5}(SO_4)_{1.25}\ (s) + 4Na^+ + 10.75(SO_4)^{2-} + 17.5H^+ \quad (1)$$

The amounts of sodium ions in solutions at the beginning of HC experiments (about 11,495 ppm) were very high compared with the amounts (about 6274 ppm) in the solution after one day of aging (Table 1). As also observed in Table 1, the decreases of Na in HC experiments is considerably higher (about 43%) than those observed in the LC experiments (about 17%). Although the analytical results do not provide direct information about the mechanism of captivation of ions, it seems clear that the incorporation of sodium ions onto schwertmannite is rather broad in HC experiments. There is little information on the mechanism of cation incorporation in the structure of this metastable phase and most studies are mainly focused on oxyanions such as arsenic, chromate and molybdate forms [10,39]. During the formation of schwertmannite, sodium can be incorporated into the structure by Fe(III) substitution or absorbed onto its surface. The substitution of Fe (III) ions by monovalent cations seem not be favourable, however, the adsorption of Na+ could be explained by the presence of surface hydroxyl groups inherent to the mineral formula ($Fe_8O_8(OH)_{5.5}(SO_4)_{1.25}$). Antelo et al. [41] studied the effect of Cu(II) incorporation into schwertmannite on the stability of this metastable phase and propose that the absorption of Cu(II) into the structure during coprecipitation processes, increases the stability of schwertmannite and decreases its transformation with respect to goethite in long

term experiments. As exposed above, a relatively rapid transformation of Na-schwertmannite into natrojarosite are observed in the present study. The incorporation of Na, with a high ionic radius (r = 102 pm) may eventually distort and destabilize the structure of the metastable phase, with a subsequent decrease in particle size. Because of this grinding, the surface to volume ratio will be higher than those of larger particles of natrojarosite, which produce an increases of the total surface free energy and hence, an increase of the solubility of the smallest particles of schwertmannite. At the same time as the dissolution of schwertmannite occurs, the larger particles of natrojarosite grow at the expense of the smaller ones by Ostwald ripening processes. However, further investigation is required to establish the details of such phenomenon. In addition, schwertmannite dissolution involves an increase of aqueous solution acidity, which improve the stability for natrojarosite precipitation according to Bigham and Nordstrom [42]. In such conditions, the dissolution of schwertmannite and the concomitant natrojarosite precipitation could be envisaged as a solvent-mediated reaction according to:

$$Fe_8O_8(OH)_{5.5}(SO_4)_{1.25}\ (s) + 2Na^+ + 2.75(SO_4)^{2-} + 9.5H^+ \rightarrow 2NaFe_3(SO_4)_2(OH)_6\ (s) + 3H_2O \quad (2)$$

3.4. Thermal Decomposition of Schwertmannite and Natrojarosite

Figure 4 displays TG, DTG and MS curves recording the ion current associated with masses 18 (H_2O), 48 (SO) and 64 (SO_2) released from representative samples of natrojarosite and schwertmannite-like compounds precipitated at ambient temperature. The TG curves exhibit a similar profile with total weight loss of 39.90% and 41.51% obtained for the low crystalline and high crystalline samples respectively at the end of the TG analyses (1000 °C). As can be observed, the decomposition occurs in three separated stages and the addition of MS curves fits the DTG curves in both samples. However, a detailed study of the DTG and MS curves confirm differences between the two phases, such as ranges of temperature, maximum weight-loss rate and distribution of chemical species in these solids. In the case of schwertmannite (Figure 4a), a first mass loss (~11%) occurs over the 25–190 °C temperature range (with a maximum weight-loss rate at ~120 °C) and derives from the release of loosely bound chemisorbed water (see blue MS curve) from the sample. A second stage (190–400 °C) with a maximum weight-loss rate at 290 °C, involves a loss ~8.3%, which is assigned to the release of hydroxyl groups. Regardless of the structural position of both water molecules and hydroxyls are not well defined [39], the results obtained here suggest that a weak hydrogen bonding network and possibly, a steady distribution of the positive charges favour an early release of water and hydroxyl groups from the low crystalline phase. DTG curves obtained here for schwertmannite are very similar to that reported by Kim et al. [43], who found a similar total weight loss at 400 °C (~21%) for a natural schwertmannite.

In the case of natrojarosite, the thermal behaviour is rather different during these two first stages. In the interval between 25–190 °C shows a minor weight loss (~2%), while an important weight loss (~13%) proceeds at slightly high temperatures (280–480 °C). Thus, only trace to minor amounts of water loss at temperature lower than 200 °C were detected in natrojarosite, which is indicative of the absence of H_3O^+ in jarosite [44]. These results (see TG and MS curves in Figure 4b) confirm the XRD results indicating that hydronium substitution in alkali positions would be negligible in natrojarosite obtained after aging in HC experiments. On the other hand, the second weight loss (maximum weight-loss rate at ~410 °C) is assigned to dexydroxylation [45]. Hydroxyl groups coordinate iron octahedral forming layers parallel to 001 plane [46] and participate in the hydrogen bonding network in the crystal structure. These crystallographic features determine the stability of the crystal structure and explain the different stages of weight loss observed between schwertmannite and natrojarosite (Figure 4a,b). The final weight loss (500–1000 °C) with a maximum rate at ~710 °C shows a loss of ~20% that is clearly attributed to the release of sulphur oxides in both samples (see green curves in Figure 4a,b).

Overall, the study of these curves (TG, DTG and MS) indicates that the weight loss observed in both the low crystalline and the high crystalline phases is due to the release of water molecules,

hydroxyl groups and sulphur as SO and SO_2 from the sulphate groups. Although both samples seem to have a similar composition, the water molecules and/or hydroxyl groups loosely bound predominates in schwertmannite while the hydroxyl group strongly attached to the crystal structure prevails in natrojarosite. Therefore, the comparison of thermal behaviour of the precipitates obtained at ambient temperature provides supplementary information on the distribution of chemical species in both schwertmannite ($Fe_8O_8(OH)_{5.5}(SO_4)_{1.25}$) and natrojarosite ($NaFe_3(SO_4)_2(OH)_6$). Moreover, TG/DTG/MS results confirm the dependence of thermal decomposition of jarosites not only upon the composition [47–49], but also upon the degree of crystallinity as described for other hydroxylsulphates (ettringite) by Jimenez and Prieto [50]. Finally, the thermogravimetric results confirm the XRD results showing similitudes between natrojarosite obtained by precipitation and pure natural natrojarosites. These results indicate that jarosite can be considered the most abundant phase in supergene deposits that have not been affected by severe hydrothermal processes on both Earth and Martian surfaces.

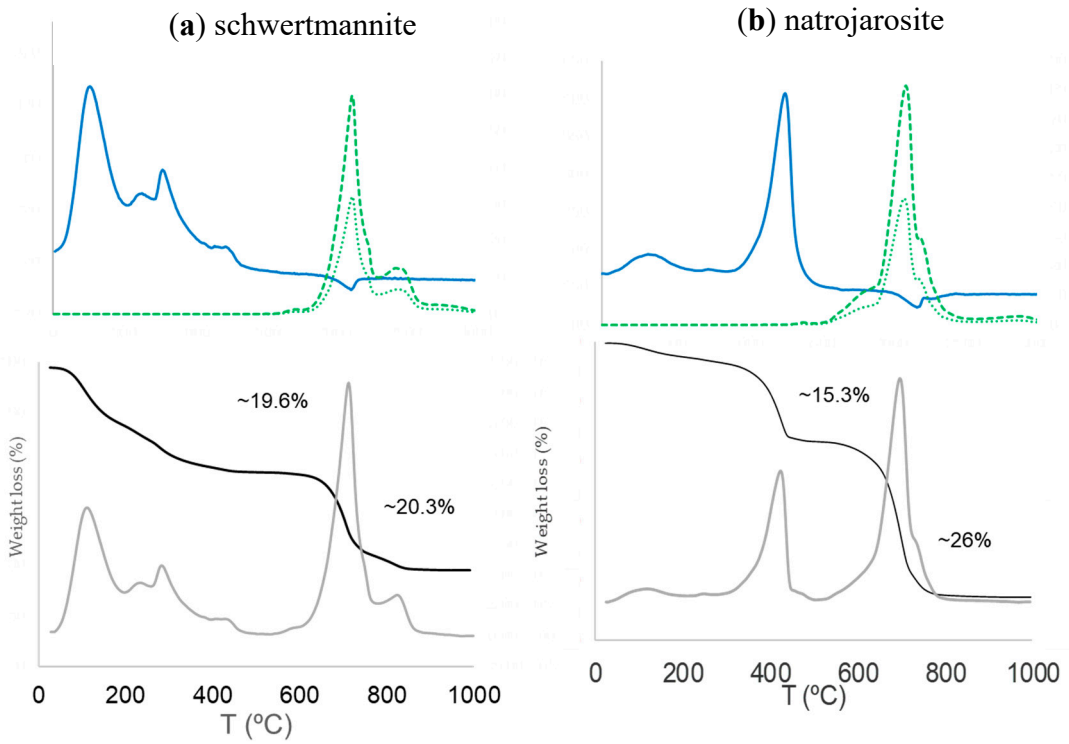

Figure 4. TG (black), DTG (grey), H_2O (blue), SO (green dotted line) and SO_2 (green dashed line) curves from representative samples of schwertmannite (**a**) and natrojarosite (**b**) obtained at the end of aging.

4. Conclusions

This experimental study shows that the complex precipitation behaviour of ferric hydroxide sulphate phases at ambient conditions is clearly influenced by the geochemistry of the parent solution. Here, the combination of XRD, SEM and EDS results indicate that schwertmannite and natrojarosite-like compounds have precipitated at highly acidic and ambient conditions after 28 days of aging in solutions with different initial concentration. A Na-schwertmannite like compound is the only phase identified in LC experiments. The incorporation of sodium ions in the crystalline structure explain the lack of typical morphology of schwertmannite and the relatively rapid transformation of schwertmannite into natrojarosite in HC experiments. The reactions involved in the transformation can be explained by Ostwald ripening processes in a solvent-mediated medium.

The study of thermal behaviour of the precipitates provides supplementary information on the distribution of chemical species in both schwertmannite ($Fe_8O_8(OH)_{5.5}(SO_4)_{1.25}$) and natrojarosite

($NaFe_3(SO_4)_2(OH)_6$). Thermal decomposition of ferric hydroxide sulphates is dependent on its composition and its degree of crystallinity as well as it shows structural similarities between precipitates and pure natural samples. The fact that the poorly crystalline phases of ferric oxide-hydroxysulphates transforms to other more crystalline phases under favourable conditions over a time scale of weeks have severe environmental effects on the mobility of metals during early diagenetic processes. The results obtained in this work improve the interpretation of the epigenetic environments where jarosite precipitates on both Earth and Martian surfaces.

Author Contributions: M.P. and A.J. designed research and interpreted results. A.J. and A.H. contributed to the experimental work. A.J. wrote the manuscript.

Funding: This work was supported by the Spanish Ministry of Economy and Competitiveness project (CGL2016-77138-C2-2-P).

Acknowledgments: This manuscript was much improved by the careful reviews of two anonymous reviews.

Conflicts of Interest: The authors declare no conflict of interest.

Abbreviations

LC	Low concentration experiment
HC	High concentration experiment
XRD	X-Ray Diffraction
SEM	Scanning Electron Microscopy
TEM	Transmission Electron Microscopy
ICP-OES	Inductive Coupling Plasma -Optical Emission Spectrometry
IC	Ion Chromatography
SI	Saturation Index
TG	Thermogravimetry
DTG	Derivate Thermogravimetry
MS	Mass Spectrometry

References

1. Cornell, R.M.; Schwertmann, U. *The Iron Oxides: Structure, Properties, Reactions, Occurrences and Uses*, 2nd ed.; John Wiley & Sons; VCH: Weinheim, Germany, 2003; p. 664.
2. Jambor, J.L.; Nordstrom, D.K.; Alpers, C.N. Metal-sulfate salts from sulfide mineral oxidation. *Rev. Mineral. Geochem.* **2000**, *40*, 303–350. [CrossRef]
3. Cornell, R.M.; Schwertmann, U. *The Iron Oxide*; VCH: New York, NY, USA, 1996; p. 377.
4. Dutrizac, J.E. The effectiveness of jarosite species for precipitating sodium jarosite. *JOM* **1999**, *51*, 30–32. [CrossRef]
5. Dutrizac, J.E.; Jambor, J.L. Jarosites and their application in hydrometallurgy. *Rev. Mineral. Geochem.* **2000**, *40*, 405–452. [CrossRef]
6. Ventruti, G.; Scordari, F.; Schingaro, E.; Gualtieri, A.F.; Meneghini, C. The order-disorder character of $FeOHSO_4$ obtained from the thermal decomposition of metahohmannite, $Fe^{3+}{}_2(H_2O)_4[O(SO_4)_2]$. *Am. Mineral.* **2005**, *90*, 679–686. [CrossRef]
7. Reddy, M.A.; Pralong, V.; Caignaert, V.; Varadaraju, U.V.; Raveau, B. Monoclinic iron hydroxy sulphate: A new route to electrode materials. *Electrochem. Commun.* **2009**, *11*, 1807–1810. [CrossRef]
8. Mohapatra, M.; Anand, S. Synthesis and applications of nano-structured iron oxides/hydroxides—A review. *Int. J. Eng. Sci. Technol.* **2010**, *2*, 127–146. [CrossRef]
9. Reich, M.; Vasconcelos, P.M. Geological and economic significance of supergene metal deposits. *Elements* **2015**, *11*, 305–310. [CrossRef]
10. Acero, P.; Ayora, C.; Torrentó, C.; Nieto, J.M. The behavior of trace elements during schwertmannite precipitation and subsequent transformation into goethite and jarosite. *Geochim. Cosmochim. Acta* **2006**, *70*, 4130–4139. [CrossRef]
11. Baron, D.; Palmer, C.D. Solubility of jarosite at 4–35 °C. *Geochim. Cosmochim. Acta* **1996**, *60*, 185–195. [CrossRef]

12. Dutrizac, J.E. The effect of seeding on the rate of precipitation of ammonium jarosite and sodium jarosite. *Hydrometallurgy* **1996**, *42*, 293–312. [CrossRef]
13. Dutrizac, J.E.; Chen, T.T. The behaviour of phosphate during jarosite precipitation. *Hydrometallurgy* **2010**, *102*, 55–65. [CrossRef]
14. Barham, J. Schwertmannite: A unique mineral, contains a replaceable ligand, transforms to jarosites, hematites, and/or basic iron sulphate. *J. Mater. Res.* **1997**, *12*, 2751–2758. [CrossRef]
15. Gagliano, W.B.; Brill, M.R.; Bigham, J.M.; Jones, F.S.; Traina, S.J. Chemistry and mineralogy of ochreous sediments in a constructed mine drainage wetland. *Geochim. Cosmochim. Acta* **2004**, *68*, 2119–2128. [CrossRef]
16. Pérez-López, R.; Asta, M.P.; Román-Ross, G.; Nieto, J.M.; Ayora, C.; Tucoulou, R. Synchrotron-based X-ray study of iron oxide transformations in terraces from the Tinto-Odiel river system: Influence on arsenic mobility. *Chem. Geol.* **2011**, *280*, 336–343. [CrossRef]
17. Bell, J.F.; McCord, T.B.; Owensby, P.D. Observational evidence of crystalline iron oxides on Mars. *J. Geophys. Res. B Solid Earth* **1990**, *95*, 14447–14461. [CrossRef]
18. Fernández-Remolar, D.C.; Morris, R.V.; Gruener, J.E.; Amils, R.; Knoll, A.H. The Río Tinto Basin, Spain: Mineralogy, sedimentary geobiology, and implications for interpretation of outcrop rocks at Meridiani Planum, Mars. *Earth Planet. Sci. Lett.* **2005**, *240*, 149–167. [CrossRef]
19. Clark, B.C. Geochemical components in Martian soil. *Geochim. Cosmochim. Acta* **1993**, *57*, 4575–4581. [CrossRef]
20. Christensen, P.R.; Bandfield, J.L.; Clark, R.N.; Edgett, K.S.; Hamilton, V.E.; Hoefen, T.; Morris, R.V. Detection of crystalline hematite mineralization on Mars by the Thermal Emission Spectrometer: Evidence for near-surface water. *J. Geophys. Res. E Planets* **2000**, *105*, 9623–9642. [CrossRef]
21. Tosca, N.J.; McLennan, S.M.; Clark, B.C.; Grotzinger, J.P.; Hurowitz, J.A.; Knoll, A.H.; Schröder, C.; Squyres, S.W. Geochemical modeling of evaporation processes on Mars: Insight from the sedimentary record at Meridiani Planum. *Earth Planet. Sci. Lett.* **2005**, *240*, 122–148. [CrossRef]
22. Christensen, P.R.; Wyatt, M.B.; Glotch, T.D.; Rogers, A.D.; Anwar, S.; Arvidson, R.E.; Fallacaro, A. Mineralogy at Meridiani Planum from the Mini-TES experiment on the Opportunity Rover. *Science* **2004**, *306*, 1733–1739. [CrossRef]
23. Rieder, R.; Economou, T.; Wänke, H.; Turkevich, A.; Crisp, J.; Brückner, J.; McSween, H.Y. The chemical composition of Martian soil and rocks returned by the mobile alpha proton X-ray spectrometer: Preliminary results from the X-ray mode. *Science* **1997**, *278*, 1771–1774. [CrossRef]
24. Burns, R.G. Gossans on mars. *Lunar Planet. Sci. Conf. Proc.* **1988**, *18*, 713–721.
25. Clark, B.C.; Van Hart, D.C. The salts of Mars. *Icarus* **1981**, *45*, 370–378. [CrossRef]
26. Parkhurst, D.L.; Appelo, C.A.J. *User's Guide to PHREEQC (Version 2): A Computer Program for Speciation, Batch-reaction, One-dimensional TRansport, and Inverse Geochemical Calculations*; US Geological Survey: Denver, CO, USA, 1999.
27. Yu, J.Y.; Heo, B.; Choi, I.K.; Cho, J.P.; Chang, H.W. Apparent solubilities of schwertmannite and ferrihydrite in natural stream waters polluted by mine drainage. *Geochim. Cosmochim. Acta* **1999**, *63*, 3407–3416. [CrossRef]
28. Carlson, L.T.; Schwertmann, U. Natural ferrihydrites in surface deposits from Finland and their association with silica. *Geochim. Cosmochim. Acta* **1981**, *45*, 421–429. [CrossRef]
29. Jambor, J.L.; Dutrizac, J.E. Occurrence and constitution of natural and synthetic ferrihydrite, a widespread iron oxyhydroxide. *Chem. Rev.* **1998**, *98*, 2549–2586. [CrossRef]
30. Bigham, J.M.; Carlson, L.; Murad, E. Schwertmannite, a new iron oxyhydroxy-sulphate from Pyhäsalmi, Finland, and other localities. *Min. Mag.* **1994**, *58*, 641–648. [CrossRef]
31. Michel, F.M.; Barrón, V.; Torrent, J.; Morales, M.P.; Serna, C.J.; Boily, J.F.; Qingsong, L.; Ambrosini, F.; Cismasu, A.C.; Brown, G.E. Ordered ferrimagnetic form of ferrihydrite reveals links among structure, composition, and magnetism. *Proc. Natl. Acad. Sci. USA* **2010**, *107*, 2787–2792. [CrossRef]
32. Bigham, J.M.; Schwertmann, U.; Traina, S.J.; Winland, R.L.; Wolf, M. Schwertmannite and the chemical modeling of iron in acid sulfate waters. *Geochim. Cosmochim. Acta* **1996**, *60*, 2111–2121. [CrossRef]
33. Caraballo, M.A.; Rimstidt, J.D.; Macías, F.; Nieto, J.M.; Hochella, M.F., Jr. Metastability, nanocrystallinity and pseudo-solid solution effects on the understanding of schwertmannite solubility. *Chem. Geol.* **2013**, *360*, 22–31. [CrossRef]
34. Regenspurg, S.; Brand, A.; Peiffer, S. Formation and stability of schwertmannite in acidic mining lakes. *Geochim. Cosmochim. Acta* **2004**, *68*, 1185–1197. [CrossRef]

35. Sanchez-España, J.; Yusta, I.; López, G.A. Schwertmannite to jarosite conversion in the water column of an acidic mine pit lake. *Min. Mag.* **2012**, *76*, 2659–2682. [CrossRef]
36. Sangwal, K. Growth kinetics and surface morphology of crystals grown from solutions: Recent observations and their interpretations. *Prog. Cryst. Growth Charact. Mater.* **1998**, *36*, 163–248. [CrossRef]
37. Carlson, L.; Bigham, J.M.; Schwertmann, U.; Kyek, A.; Wagner, F. Scavenging of As from acid mine drainage by schwertmannite and ferrihydrite: A comparison with synthetic analogues. *Environ. Sci. Technol.* **2002**, *36*, 1712–1719. [CrossRef]
38. Antelo, J.; Fiol, S.; Gondar, D.; López, R.; Arce, F. Comparison of arsenate, chromate and molybdate binding on schwertmannite: Surface adsorption vs anion-exchange. *J. Colloid Interface Sci.* **2012**, *386*, 338–343. [CrossRef]
39. Fernández-Martínez, A.; Timon, V.; Roman-Ross, G.; Cuello, G.J.; Daniels, J.E.; Ayora, C. The structure of schwertmannite, a nanocrystalline iron oxyhydroxysulfate. *Am. Mineral.* **2010**, *95*, 1312–1322. [CrossRef]
40. Sangwal, K. Kinetic effects of impurities on the growth of single crystals from solutions. *J. Cryst. Growth* **1999**, *203*, 197–212. [CrossRef]
41. Antelo, J.; Fiol, S.; Gondar, D.; Pérez, C.; López, R.; Arce, F. Cu (II) incorporation to schwertmannite: Effect on stability and reactivity under AMD conditions. *Geochim. Cosmochim. Acta* **2013**, *119*, 149–163. [CrossRef]
42. Bigham, J.M.; Nordstrom, D.K. Iron and aluminum hydroxysulfates from acid sulfate waters. *Rev. Mineral. Geochem.* **2000**, *40*, 351–403. [CrossRef]
43. Kim, J.; Kim, S.; Tazaki, K. Mineralogical characterization of microbial ferrihydrite and schwertmannite, and non-biogenic Al-sulfate precipitates from acid mine drainage in the Donghae mine area, Korea. *Environ. Geol.* **2002**, *42*, 19–31.
44. Swayze, G.A.; Desborough, G.A.; Smith, K.S.; Lowers, H.A.; Hammarstrom, J.M.; Diehl, S.F.; Leinz, R.W.; Driscoll, R.L. Chapter, B: Understanding jarosite: From mine waste to Mars. Understanding contaminants associated with mineral deposits. *US Geol. Surv. Circ.* **2008**, *1328*, 8–13.
45. Drouet, C.; Pass, K.L.; Baron, D.; Draucker, S.; Navrotsky, A. Thermochemistry of jarosite-alunite and natrojarosite-natroalunite solid solutions. *Geochim. Cosmochim. Acta* **2004**, *68*, 2197–2205. [CrossRef]
46. Kato, T.; Miúra, Y. The crystal structures of jarosite and svanbergite. *Mineral. J.* **1977**, *8*, 419–430. [CrossRef]
47. Alpers, C.N.; Nordstrom, D.; Ball, J.W. Solubility of jarosite solid solutions precipitated from acid mine waters, Iron Mountain, California, USA. *Sciences Géologiques Bulletins et Mémoires* **1984**, *42*, 281–298. [CrossRef]
48. Drouet, C.; Navrotsky, A. Synthesis, characterization, and thermochemistry of K-Na-H_3O jarosites. *Geochim. Cosmochim. Acta* **2003**, *67*, 2063–2076. [CrossRef]
49. Frost, R.L.; Weier, M.L.; Martens, W. Thermal decomposition of jarosites of potassium, sodium and lead. *J. Therm. Anal. Calorim.* **2005**, *82*, 115–118. [CrossRef]
50. Jiménez, A.; Prieto, M. Thermal stability of ettringite exposed to atmosphere: Implications for the uptake of harmful ions by cement. *Environ. Sci. Technol.* **2015**, *49*, 7957–7964. [CrossRef]